

Effect of carrier gas on mechanical properties and fracture behaviour of cold sprayed aluminium coatings

S. R. Bakshi¹, T. Laha¹, K. Balani¹, A. Agarwal^{*1} and J. Karthikeyan²

Two different coatings of 1100 aluminium were cold sprayed onto similar substrates, using He and He–20N₂ (vol.-%) mixture as carrier gases. Three point bend testing was carried out. The elastic moduli of the coatings were found to be close to each other and the substrate. The He processed coating showed higher fracture strength which was attributed to the higher degree of strain hardening. The He–20N₂ processed coating failed at lower stress owing to its strain relaxed structure. The mode 1 fracture of the coating substrate system was found to be higher for the helium processed coating. The toughness was correlated to the microstructure. The delaminated coating showed a higher degree of brittle failure of the interface for the He processed coating.

Keywords: Cold spraying, 1100 aluminium, Fracture surface, Fracture toughness, Three point bend test, Elastic modulus, Brittle fracture, Delamination, Notch, Porosity, Carrier gas, Splats, Dislocation pile up, Subgrain formation

Introduction

Cold spraying is a relatively new coating technique where metallic powder particles are accelerated to very high velocities (600–1500 m s⁻¹) by a carrier gas (He, N₂) flowing at very high pressure (up to 3.5 MPa) and impact the substrate through a converging–diverging de laval nozzle.¹ The carrier gas is preheated to a temperature between 300 and 800°C, partly in order to compensate for the cooling produced by expansion of the gas and to reduce the density which in turn increases the sonic velocity, but below the melting point of the particles. The loss of kinetic energy on impact causes plastic deformation of the particles. This process is also known as cold kinetic spraying. The low temperature solid state coating process eliminates problems owing to oxidation and defects owing to solidification. The disadvantage is that a large amount of carrier gas is lost, unless recycled, and that only plastically deformable materials can be deposited. Many materials have been deposited till date by cold spraying including pure metals,^{2–6} alloys⁷ and composite materials.^{8,9} The exact mechanism of the bonding is not fully understood. It is believed that impact of the particles results in rupture of oxide layers which provides clean surfaces for bonding. Bonding has been attributed to adiabatic shear instabilities at particle/particle and particle/substrate interfaces owing to impact and has been modelled using finite element analysis.^{10,11} The parameters affecting the process and spraying efficiency are particle size, density

of particles, temperature of gas and density of gas and spraying angle, and various models have been proposed for the effect of various parameters.^{12–14}

In the authors' earlier work,^{6,16} cold spraying of 1100 Al on 1100 Al substrate was reported. Two different carrier gases, namely He and He–20N₂ (vol.-%), were used to study the effect of carrier gas on the properties of the coating. It was observed that the 100%He processed coating had higher hardness than the He–20N₂ processed coating. TEM analysis revealed dislocation pile-ups and oxide layers in the He processed coating. The He–20N₂ processed coating showed subgrain formation and a relaxed structure.¹⁶ There was more strain hardening in the He processed coating as compared with He–20N₂ processed coatings. Potentiodynamic polarisation experiments in 0.9 pH H₂SO₄ revealed that the corrosion current density was higher for the He processed coating than for the He–20N₂ processed coating indicating superior corrosion resistance of the He–20N₂ processed coating.⁶

The purpose of the present work is to study the effect of the carrier gas on the fracture strength and interfacial properties of the coating/substrate and to establish correlation with the microstructure. Three point bend testing of the samples was carried out. The elastic modulus and fracture properties were studied.

Experimental

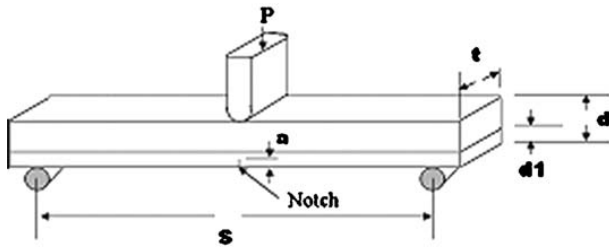
The schematic of the three point bend test is shown in Fig. 1. A notch was introduced at the midpoint of the specimen using a diamond saw. The initial crack length was measured by optical microscopy of the cross-section. Table 1 tabulates the dimensions of the samples used.

For the three point bend test geometry the elastic modulus of the coating/substrate system is given by the

¹Research Student, Department of Mechanical and Materials Engineering, Florida International University, Miami, FL, USA

²Director of Research and Development, ASB Industries, Barberton, OH, USA

*Corresponding author, email agarwala@fiu.edu



1 Schematic of three point bend test

modified equation¹⁷

$$E_{\text{coating/substrate}} = \frac{S^3}{4t(d-a)^3} \left(\frac{dP}{dx} \right) \quad (1)$$

where dP/dx is the slope of the linear portion of the load deflection curve and all symbols indicating the dimensions are shown in Fig. 1 and Table 1.

2 The elastic modulus of the coating can be computed from the 'rule of mixtures' (ROM) equation¹⁷

$$E_{\text{coating/substrate}} = E_{\text{coating}} V_c + E_{\text{substrate}} (1 - V_c) \quad (2)$$

where V_c is the volume fraction of the coating.

The apparent mode I fracture toughness and critical strain energy release rate were calculated using equations (3)–(5) (Ref. 18)

$$K_{\text{IC}}^{\text{app}} = \left(\frac{P_{\text{max}} S}{td^{1.5}} \right) f(r) \quad (3)$$

where $r = \frac{a}{d}$ and P_{max} is the load at the intersection of the line with slope equal to 0.95 times the slope of the linear part of the load deflection curve, and the load deflection curve

$$f(r) = 3(r)^{1/2} \left[\frac{1.99 - r(1-r)(2.15 - 3.93r + 2.7r^2)}{2(1+2r)(1-r)^{1.5}} \right] \quad (4)$$

$$G_c = \frac{K_c^2 (1 - \nu^2)}{E} \quad (5)$$

Scanning electron microscopy was performed on the fracture surface perpendicular to the coating as well as the delaminated surface to study and compare the failure behaviour of the coating as well as the interface.

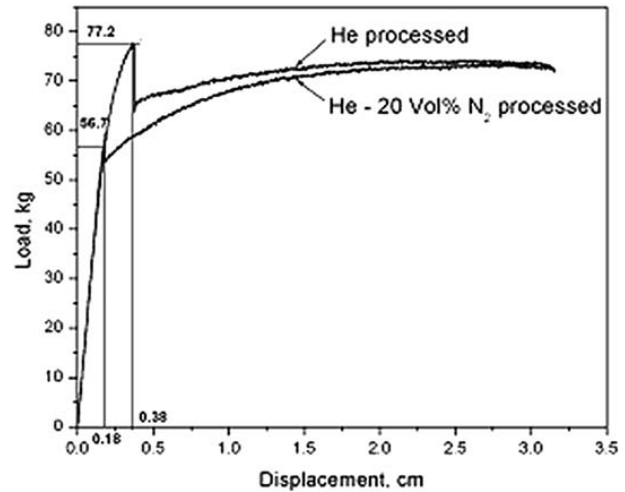
Results and discussion

Three point bend test

Figure 2 shows the load deflection curves for the 100%He and He–20N₂ processed coatings. It can be seen that the slope of the load deflection curve for the 100%He and He–20N₂ processed coatings are almost identical indicating that they have similar elastic moduli. The measured values of the elastic modulus 100%He

Table 1 Dimension of test specimen

Dimension	He processed specimen	He–20N ₂ processed specimen
Span S, mm	131	131
Width t, mm	16.2	16
Depth d, mm	5.6	5.9
Coating thickness d ₁ , μm	1200	1000
Crack length a, μm	108	318



2 Load deflection curve obtained by three point bend test for 100%He and He–20N₂ processed 1100 aluminium coatings

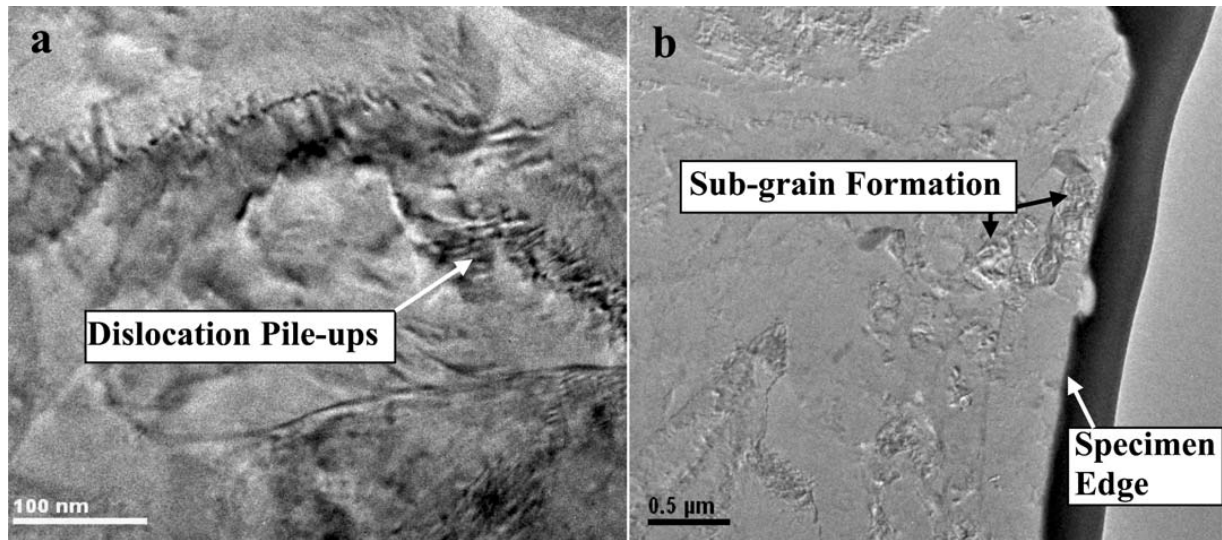
processed coating and He–20N₂ processed coating are 69.1 and 68.7 GPa respectively. In the authors' earlier paper⁶ the specific gravities of the 100%He processed coating and He–20N₂ processed coating were measured as 2.63 and 2.52 respectively. Taking the true density of 1100 Al¹⁹ as 2.71, this corresponds to a porosity of 3 and 7% respectively for the 100%He processed coating and He–20N₂ processed coating.

Using the classical rule of mixtures for calculating elastic modulus of composites and assuming a value of 0 for the elastic modulus of porosity, the following equation can be drawn

$$E_{\text{Porous}} = E_{100\% \text{Dense}} \left(\frac{\rho_{\text{Porous}}}{\rho_{100\% \text{Dense}}} \right) \quad (6)$$

where E stands for elastic modulus and ρ is the density of the material. Using equation (6) and taking the value of $E_{100\% \text{Dense}}$ for 1100 Al as 69 GPa (Ref. 19), the elastic moduli of the 100%He processed and He–20N₂ processed coatings are found to be 66.9 and 64.2 GPa respectively. Using equation (2) the values of the $E_{\text{coating/substrate}}$ for 100%He processed and He–20N₂ processed coatings are found to be 68.6 and 68.2 GPa respectively. It is seen that the difference in elastic modulus of the coatings does not lead to a significant difference in elastic modulus of the coating/substrate system. The difference in the elastic modulus is within the error limits of the measurement and cannot be resolved properly.

It is seen that the load increases with deflection. As the crack reaches the interface, delamination occurs and the crack propagates along the interface. There is a decrease in the load owing to the decrease in load bearing thickness after delamination. The 100%He processed coating fails at higher load indicating that it is stronger. The large reduction in load for the 100%He processed coating indicates that the interface failed in a brittle manner. There is a very small decrease in load when the He–20N₂ coating fails indicating somewhat cohesive failure of the coating and interface. It also indicates a tougher interface for the He–20N₂ processed coating. From Fig. 2 the apparent mode I fracture toughness was calculated and is tabulated in Table 2 below.



3 Images (SEM) of a He processed and b He-20N₂ processed coatings

Figure 3 shows the TEM images of the two coatings. Extensive dislocation pile-ups are seen in the strain hardened structure of the helium processed coating whereas the subgrain formation in He-20N₂ processed coating indicates the strain relaxed structure. The higher strength of the 100%He processed coating is evident from the fact that the degree of strain hardening is higher owing to the higher speed attained by the particles in helium and the presence of oxide.¹⁶ The He-20N₂ processed coating has a lower fracture strength which is attributed to the relatively strain relaxed structure of the coating owing to subgrain formation.¹⁶

The apparent fracture toughness of the He processed coating (4.2 MPa m^{1/2}) is less than that of the He-20N₂ processed coating (6.5 MPa m^{1/2}). This can be explained by the fact that degree of cold work is higher in the 100%He processed coating making it more brittle.

SEM characterisation of fracture surface

SEM was carried on the fracture surface perpendicular to the coating and the delaminated surface of the coating. Figure 4 shows a schematic of the specimen after the three point bend test and the surfaces examined in SEM.

Figure 5 shows the SEM of the fracture surface perpendicular to the coatings whereas Fig. 6 shows the SEM of the delaminated surface of the coatings. It can be seen from Fig. 5 that the crack starts growing from the notch and propagates owing to failure of successive splats. It is evident that the splats have undergone more compaction to form a denser microstructure in the He processed coating (Fig. 5a) than the He-N₂ processed

coating (Fig. 5b). As seen along the interface of the notch and cracked surface, continuity of splat fracture is observed in the He processed coating whereas stretching of splats into a stepped structure is observed in the He-20N₂ coating.

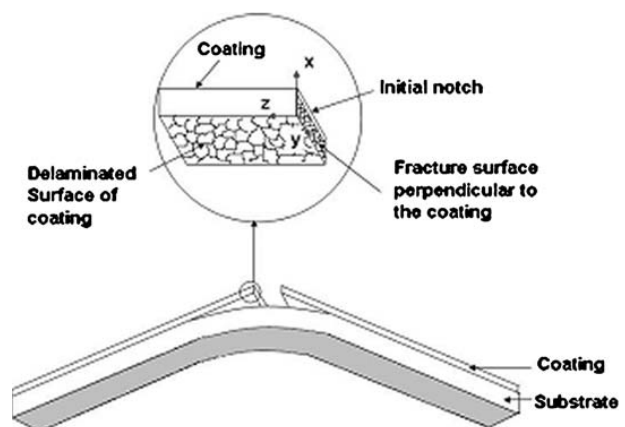
This step structure indicates a higher value of energy absorption during fracture similar to failure of a layered configuration producing a higher G_c value for the He-N₂ processed coating. Finally, when the crack reaches the coating/substrate interface, it propagates along the coating/substrate interface. Figure 6 shows the SEM image of the delaminated surface of the coating.

It is observed that the delamination crack moves at ~45° to the length of the coating for the helium processed coating while it is less defined in the He-20N₂ processed coating. Also, the delaminated surface of the He processed coating is relatively flatter than that of the He-20N₂ processed coating indicating a lower degree of plastic deformation of the interface during crack propagation for the He processed coating.

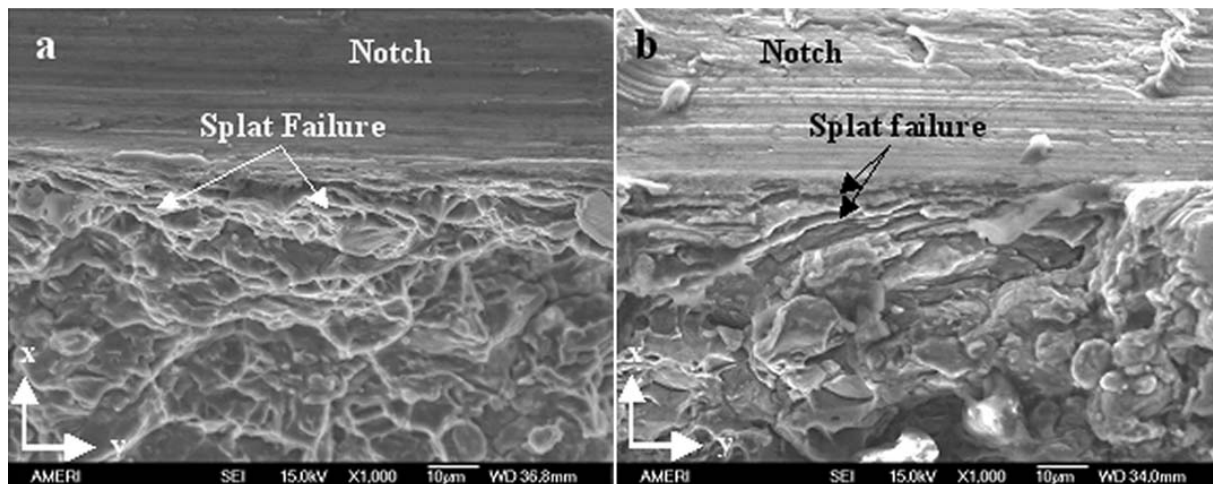
It is inferred from Fig. 6 that the interface is less tough for the He processed coating. This is due to the fact that the particle velocity is higher in helium as compared with a mixture of He-20N₂. Therefore the amount of plastic deformation undergone by the particles and the substrate surface, which is due to loss

Table 2 Mechanical properties of coatings

Property	He processed	He-20N ₂ processed
Slope, N m ⁻¹	3.3 × 10 ⁵	3.4 × 10 ⁵
P_{max} , N	549	555
Load at delamination, N	757	556
$r = a/d$	0.019	0.054
$E_{coating/substrate}$, GPa	69.1	68.7
Apparent K_{IC} of coating/substrate, MPa m ^{1/2}	4.2	6.5
G_c , J m ⁻²	232	546

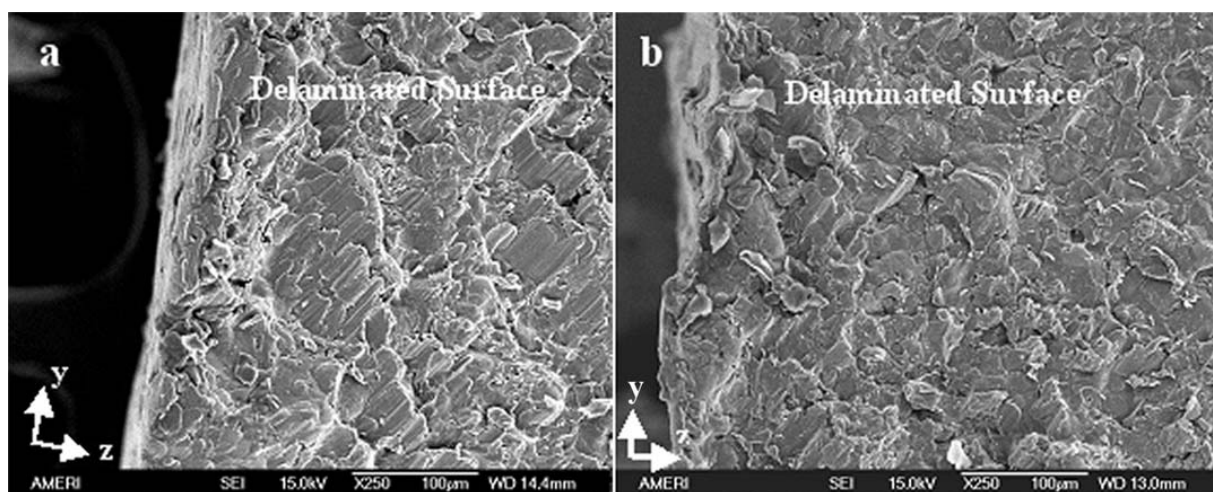


4 Schematic of specimen after three point bend test and fracture surfaces examined in SEM



a 100%He processed; b He-20N₂ processed

5 Images (SEM) of fracture surface perpendicular to coating



a 100%He processed; b He-20N₂ processed

6 Images (SEM) of delaminated surface of coating

of kinetic energy on impact, is greater for the He processed coating. So the resulting interface is more strain hardened and brittle for the He processed coating.

Conclusions

Three point bend testing was carried out on the cold sprayed coatings produced using He and He-20N₂ as carrier gases. The 100%He coating fails at higher load than the coating formed by He-20N₂. There is a significant decrease in load after delamination in the 100%He processed coating whereas that is small for the He-20N₂ processed coating. Delamination occurs by brittle failure of the interface in the 100%He processed coating whereas in case of He-20N₂ processed coating the coating and substrate deformed congruently (cohesive failure) without sudden delamination. The coating/substrate interface is stronger for the He-20N₂ processed coating. The higher fracture strength of the 100%He processed coating can be attributed to the higher degree of strain hardening owing to higher velocity of particles in helium. The relaxation of stresses in the He-20N₂ processed coating owing to subgrain formation may be reducing the level of strain hardening and hence the strength of the coating. The elastic

modulus was found to be almost the same for both the coatings which in turn was equal to that of the substrate. The apparent K_{IC} values suggest that the fracture toughness of the He-20N₂ processed coating/substrate system (6.5 MPa m^{1/2}) is better than the He processed coating/substrate system (4.2 MPa m^{1/2}). SEM of delaminated surface shows a higher degree of brittle fracture in the 100%He processed coating as compared with the He-20N₂ coating.

Acknowledgements

The authors wish to acknowledge Mr Amit Datye in Department of Mechanical and Materials Engineering at Florida International University (FIU) for his help in three point bend test. Mr Tapas Laha and Mr Kantesh Balani would like to acknowledge the Dissertation Year Fellowship Award from FIU.

References

1. United States Patent 5302414, 1994.
2. C. Borchers, F. Garner, T. Stoltenhoff and H. Kreye: *J. Appl. Phys.*, 2004, **96**, (8), 4288-4292.
3. T. H. Van Steenkiste, J. R. Smith, R. E. Teets, J. J. Moleski, D. W. Gorkeiwicz, R. P. Tyson, D. R. Marantz, K. A. Kowalsky, W. L.

- Riggs, II, P. H. Zajchowski, B. Pilsner, R. C. McCune and K. J. Barnett: *Surf. Coat. Technol.*, 1999, **111**, 62–71.
4. A. V. Bolesta, V. M. Fomin, M. R. Sharafutdinov and B. P. Tolochko: *Nucl. Instr. Meth. Phys. Res. A*, 2001, **470A**, 249–252.
 5. C. J. Li, W. Y. Li and Y. Y. Wang: *Surf. Coat. Technol.*, 2005, **198**, 469–473.
 6. K. Balani, T. Laha, A. Agarwal, J. Karthikeyan and N. Munroe: *Surf. Coat. Technol.*, 2005, **195**, 272–279.
 7. L. Ajdelsztajn, A. Zuniga, B. Jodoïn, and E. J. Lavernia: *Surf. Coat. Technol.*, to be published in 2005.
 8. H. K. Kang and S. B. Kang: *Scr. Mater.*, 2003, **49**, 1169–1174.
 9. H. J. Kim, C. H. Lee and S. Y. Hwang: *Mater. Sci. Eng. A*, 2005, **A391**, 243–248.
 10. M. Grujicic, C. L. Zhao, W. S. DeRosset and D. Helfritsch: *Mater. Des.*, 2004, **25**, 681–688.
 11. H. Assadi, F. Gartner, T. Stoltenhoff and H. Kreye: *Acta Mater.*, 2003, **51**, 4379–4394.
 12. V. Champagne, D. Helfritsch, P. Leyman, R. Lempicki and S. Grendahl: *Modell. Simul. Mater. Sci. Eng.*, 2005, **13**, 1119–1128.
 13. M. Grujicic, C. L. Zhao, W. S. DeRosset and D. Helfritsch: *Mater. Sci. Eng. A*, 2004, **A368**, 222–230.
 14. C. J. Li, W. Y. Li, Y. Y. Wang, G. J. Yang and H. Fukanuma: *Thin Solid Films*, 2005, **498**, 79–85.
 15. T. H. Van Steenkiste, J. R. Smith and R. E. Teets: *Surf. Coat. Technol.*, 2002, **154**, 237–252. 4
 16. K. Balani, A. Agarwal, S. Seal and J. Karthikeyan: *Scr. Mater.*, 2005, **53**, 845–850.
 17. N. E. Dowling: 'Mechanical behavior of materials: engineering methods for deformation, fracture, and fatigue', 1st edn, 129, 191–192; 1993, Upper Saddle River, NJ, Prentice Hall.
 18. T. R. Guess, E. D. Reedy and M. Stavig: 'Mechanical properties of hysol EA-9394 structural adhesive', Sandia Report SAND95-0229.UC-704, Albuquerque, NM, USA, 1995.
 19. J. R. Davis (ed.): 'ASM specialty handbook: aluminium and aluminium alloys'; 1993, Materials Park, OH, ASM International.

Authors Queries

Journal: **Surface Engineering**

Paper: **408**

Title: **Effect of carrier gas on mechanical properties and fracture behaviour of cold sprayed aluminium coatings**

Dear Author

During the preparation of your manuscript for publication, the questions listed below have arisen. Please attend to these matters and return this form with your proof. Many thanks for your assistance

Query Reference	Query	Remarks
1	Author: please confirm the short title.	
2	Author: should the reference no. be 17?	
3	Author: is the change OK?	
4	Author: please cite Ref. 15 in the text.	